A Model for Doubly Clamped Piezoelectric Energy Harvesters With Segmented Electrodes

Richik Kashyap, T. R. Lenka, *Member, IEEE*, and Srimanta Baishya, *Member, IEEE*

***Abstract*— An analytical model for doubly clamped piezoelectric energy harvesters with segmented electrodes, considering the effect of strain nodes formation and charges cancellation issues, is presented. The single-mode power and voltage outputs of each of the lead zirconate titanate segments are obtained and are connected in series across a resistive load for the total outputs. The analytical solutions are found to closely agree with the Finite Element Method (FEM) simulation results obtained from COMSOL Multiphysics.**

***Index Terms*— Doubly clamped beams, Euler-Bernoulli beam, piezoelectric energy harvester, segmented electrodes, strain nodes.**

I. Introduction

NOWADAYS, vibration-based energy harvesters are very promising solutions to meet the unlimited demands of power supplies for microelectronic components. Traditional chemical batteries are bulky, need periodic maintenance, have limited lifetime, and hazardous to environment. Energy harvesters can be suitable substitutes for chemical batteries used in wireless sensors, Un-manned air vehicles (UAV), and many electronically operated automated systems working in robust environments. In practice, there exist three vibration based energy harvesting mechanisms viz. piezoelectric [1]–[12], electrostatic [13], and electromagnetic [14]; among which the piezoelectric transduction is widely acknowledged [2]. They have larger power densities, simpler geometry, and can easily be integrated with micro-scale electronic devices using thin film fabrication technologies. Moreover, the piezoelectric harvesters have comparatively higher voltage levels and unlike electrostatic harvesters [8], they do not require any external voltage input. The doubly clamped piezoelectric harvesters are becoming increasingly important due to its uniform stress distribution along the entire beam compared to cantilevered structures [3], where the stress is maximum at its fixed end. We know that there are strain nodes at all modes of vibrations in doubly clamped harvesters and also at higher modes for cantilevered harvesters. The use of continuous electrodes covering the strain nodes decreases their efficiency [4]. Therefore, for better power efficiency, the segmented electrode harvesters are likely to be the future harvesters. Most of the developed cantilevered harvester models [5], [8]–[10] and doubly clamped harvester model [12] are based on continuous electrodes. Thus, we require an accurate model for piezoelectric harvesters (cantilevered and doubly clamped) that can predict the outputs of segmented electrode harvesters.

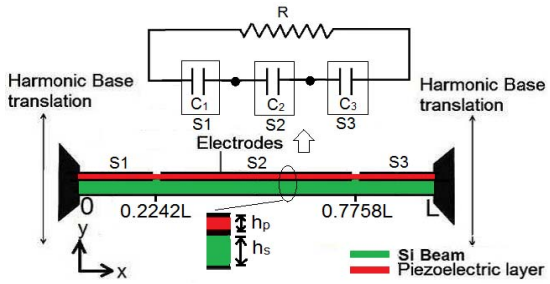

Fig. 1. Doubly clamped d_{31} mode piezoelectric energy harvester showing a series connection of capacitors of the segmented electrodes across a load.

Various modeling approaches available in the literature to model the outputs of nonsegmented harvesters include: lumped parameter modeling [6], Rayleigh–Ritz discretized model [7], and models based on Galerkin discretization [5], [10]–[11]. All these models ignore the effect of strain nodes.

Here, we present an exact analytical solution of a doubly clamped unimorph segmented harvester. The model uses a reduced order and is based on the Galerkin discretizations along with the Euler-Bernoulli beam assumptions.

II. Model Description

As shown in Fig. 1, we have considered a Si beam fully covered with a lead zirconate titanate (PZT) layer, operated in d_{31} mode and having a length of L. The material properties of PZT used are same as given in [5]. The governing equation for the free vibrations of an undamped and uniform Euler-Bernoulli beam is given by [8]–[9], [15], [16]:

$$YI\partial^4 w(x,t)/\partial x^4 + m\partial^2 w(x,t)/\partial t^2 = 0 \tag{1}$$

where YI is the bending stiffness, m is the mass per unit length, and $w(x,t)$ is the absolute transverse displacement of the beam at time t and location x along the length of the beam. The absolute transverse displacement of the beam is given by [8], [9], [15]:

$$w(x,t) = w_b(x,t) + w_{rel}(x,t) \tag{2}$$

where w_b is the base motion and w_{rel} is the transverse displacement relative to fixed end. Considering the effects of strain rate and damping mechanisms [5], [8], [9] and using (1)-(2), we obtain the partial differential equation

Manuscript received September 26, 2015; revised October 22, 2015; accepted October 24, 2015. Date of publication October 29, 2015; date of current version November 20, 2015. The review of this letter was arranged by Editor S. Pourkamali.

The authors are with the Department of Electronics and Communication Engineering, National Institute of Technology at Silchar, Silchar 788010, India (e-mail: rknits2010@gmail.com).

Color versions of one or more of the figures in this letter are available online at http://ieeexplore.ieee.org.

Digital Object Identifier 10.1109/LED.2015.2496186

governing the vibration of the doubly clamped harvester and is given by:

$$YI\partial^4 w(x,t)/\partial x^4 + c_s I\partial^5 w_{rel}(x,t)/\partial x^2\partial t + c_a\partial w_{rel}(x,t)/dt = -m\partial^2 w_b(x,t)/\partial t^2 - c_a\partial w_b(x,t)/dt - m\partial^2 w_{rel}(x,t)/\partial t^2 \quad (3)$$

where c_s and c_a, respectively, are the strain rate and viscous air damping coefficients and m is the mass per unit length of the beam. The doubly clamped unimorph harvester is subjected to uniform harmonic base translation vibration $g(t)$ at both its fixed ends, and hence, we have $w_b(x,t) = g(t)$ [8]. The internal bending moment $M(x,t)$ of the composite structure is given by [5]:

$$M(x,t) = -b\left(\int_{h_a}^{h_b}\sigma_3^s y dy + \int_{h_b}^{h_c}\sigma_3^p y dy\right) \quad (4)$$

where b is the breadth of the beam, h_a and h_b, are the positions of the bottom and top of the Si layer from the neutral axis, respectively, h_c is the position of the top of the PZT layer from the neutral axis, and σ_3^s and σ_3^p are the stresses developed in Si beam and PZT layer, respectively. To avoid the charge cancellation in fundamental mode, three electrode pairs are planted separately in the regions: $0 \le x < 0.2242L$, $0.2242\text{L} \le x < 0.7758L$, and $0.7758L \le x \le L$ [4]. Considering these regions of segmented electrodes and following the usual substitution method [5] of the piezoelectric constitutive equations and bending strain terms in the internal moment equation, we have:

$$\begin{aligned} M(x,t) = {} & YI\partial^2 w_{rel}/\partial x^2 + \vartheta V_1(t)[H(x) - H(x - x_a)] \\ & + \vartheta V_2(t)[H(x - 0.2242L) - H(x - x_b)] \\ & + \vartheta V_3(t)[H(x - 0.7758L) - H(x - L)] \end{aligned} \quad (5)$$

where $H(x)$ is the Heaviside function, V_1, V_2, and V_3 are the voltages generated across the capacitors of the first, second, and third segments, respectively, x_a and x_b correspond to some arbitrary values just less than 0.2242L and 0.7758L, respectively. The parameters YI and ϑ have similar expressions and meanings [5]. Using Galerkin discretization, we can express the relative transverse displacement as a convergent summation series contributed by every possible vibration modes associated with the beam [5], [10], [11]:

$$w_{rel}(x,t) = \sum_{r=1}^{\infty}\varphi_r(x)\eta_r(t) \quad (6)$$

where φ_r and η_r, respectively, are the mode shapes and modal coordinates of the beam for the r$^{\text{th}}$ mode. Contributions from all the vibration modes of the harvester are included in (6). But the vibratory response of a beam under modal excitation at any r$^{\text{th}}$ mode is primarily contributed by the r$^{\text{th}}$ term only [8]. For a doubly clamped beam, φ_r is given by [16], [17]:

$$\varphi_r(x) = \sqrt{\frac{1}{mL}}\left\{cosh\frac{\lambda_r}{L}x - cos\frac{\lambda_r}{L}x - \left(\frac{cos\lambda_r - cosh\lambda_r}{sin\lambda_r - sinh\lambda_r}\right) \times \left(sinh\frac{\lambda_r x}{L} - sin\frac{\lambda_r x}{L}\right)\right\} \quad (7)$$

where λ_r is a dimensionless parameter obtained from the following characteristic equation [16], [17]:

$$cos\lambda_r + \cosh\lambda_r = 1 \quad (8)$$

Substituting (6) in (3) and using the orthogonality conditions [5], [16], the corresponding coupled equation is given by:

$$d^2\eta_r/dt^2 + 2\zeta_r\omega_r d\eta_r/dt + \omega_r^2\eta_r + \chi_{r1}V_1 + \chi_{r2}V_2 + \chi_{r3}V_3 = N_r(t) = -md^2g/dt^2\int_0^L\varphi_r dx \quad (9)$$

where the backward coupling factors are:

$$\chi_{r1} = \vartheta d\varphi_r/dx\big|_{x_a} \quad (10)$$

$$\chi_{r2} = \vartheta\left[d\varphi_r/dx\big|_{x_b} - d\varphi_r/dx\big|_{0.2242L}\right] \quad (11)$$

$$\chi_{r3} = -\vartheta d\varphi_r/dx\big|_{0.7758L} \quad (12)$$

and, ζ_r and ω_r are mechanical damping ratio and undamped natural frequency of the r$^{\text{th}}$ mode, respectively, and have similar expressions [5]. Using Gauss's law, piezoelectric constitutive relations [5], and (6) we have three electrical circuit equations for each of the capacitors in the three segmented regions, and are given by:

$$\left(\epsilon_{33}bx_a/h_p\right)(dV_1/dt) + V_1/R = \sum_{r=1}^{\infty}K_{r1}d\eta_r/dt \quad (13)$$

$$\frac{\epsilon_{33}b(x_b - 0.2242L)}{h_p}\frac{dV_2}{dt} + \frac{V_2}{R} = \sum_{r=1}^{\infty}K_{r2}\frac{d\eta_r}{dt} \quad (14)$$

$$\frac{\epsilon_{33}b(L - 0.7758L)}{h_p}\frac{dV_3}{dt} + \frac{V_3}{R} = \sum_{r=1}^{\infty}K_{r3}\frac{d\eta_r}{dt} \quad (15)$$

where

$$K_{r1} = -Y_p d_{31}h_{pc}b\, d\varphi_r/dx|_{x_a} \quad (16)$$

$$K_{r2} = -Y_p d_{31}h_{pc}b\left[d\varphi_r/dx|_{x_b} - d\varphi_r/dx|_{0.2242L}\right] \quad (17)$$

$$K_{r3} = Y_p d_{31}h_{pc}b\, d\varphi_r/dx|_{0.7758L} \quad (18)$$

are the forward coupling factors for each of the respective regions, $Y_p, \epsilon_{33}, d_{31}$, and h_{pc} are the elastic modulus, permittivity at constant strain, piezoelectric strain constant, and distance of center of piezoelectric layer to the neutral axis [5], respectively. Assuming linearity and harmonic base excitations at a driving angular frequency ω, we can assume $g = G_0e^{j\omega t}$, $N_r = N_{r0}e^{j\omega t}$, $\eta_r = \eta_{r0}e^{j\omega t}$, $V_1 = V_{m1}e^{j\omega t}$, $V_2 = V_{m2}e^{j\omega t}$, $V_3 = V_{m3}e^{j\omega t}$, where G_0, N_{r0}, η_{r0}, V_{m1}, V_{m2}, and V_{m3} are the amplitudes of the respective functions. With these assumptions and neglecting the summation terms to obtain the single-mode solutions, we can express (9) and (13)-(15) as:

$$\eta_{r0}\left(\omega_r^2 - \omega^2 + j2\zeta_r\omega_r\omega\right) + \chi_{r1}V_{m1} + \chi_{r2}V_{m2} + \chi_{r3}V_{m3} = N_{r0} \quad (19)$$

$$V_{m1}\left(1/R + j\omega C_1\right) = j\omega K_{r1}\eta_{r0} \quad (20)$$

$$V_{m2}\left(1/R + j\omega C_2\right) = j\omega K_{r2}\eta_{r0} \quad (21)$$

$$V_{m3}\left(1/R + j\omega C_3\right) = j\omega K_{r3}\eta_{r0} \quad (22)$$

where $C_1 = \epsilon_{33}bx_a/h_p$, $C_2 = \epsilon_{33}b(x_b - 0.2242L)/h_p$, and $C_3 = \epsilon_{33}b(L - 0.7758L)/h_p$ are capacitances of segmented electrodes for the segments S1, S2, and S3, respectively.

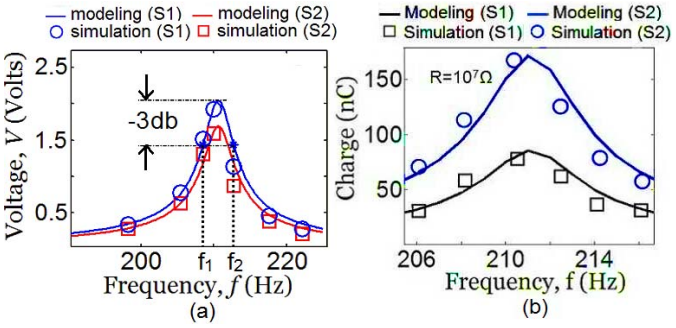

Fig. 2. Variation of (a) Voltages across capacitors and (b) Capacitor charges with frequency in S1 and S2 under open circuit.

Using (19)-(22), we get:

$$\eta_{r0} = \frac{N_{r0}}{\omega_r^2 - \omega^2 + j2\zeta_r\omega_r\omega + \frac{j\omega K_{r1}\chi_{r1}}{1/R+j\omega C_1} + \frac{j\omega K_{r2}\chi_{r2}}{1/R+j\omega C_2} + \frac{j\omega K_{r3}\chi_{r3}}{1/R+j\omega C_3}} \tag{23}$$

The reduced single mode individual voltage magnitudes for each of three capacitors in segmented regions across a resistance R can be obtained by substituting η_{r0} in (20)-(22). The sinusoidal single mode voltage expression for the ith (i=1, 2, 3) segment electrode is obtained as:

$$V_i(t) = \frac{j\omega K_{ri} N_{r0} e^{j\omega t}\left(1/R + j\omega C_i\right)^{-1}}{\omega_r^2 - \omega^2 + j2\zeta_r\omega_r\omega + \frac{j\omega K_{r1}\chi_{r1}}{1/R+j\omega C_1} + \frac{j\omega K_{r2}\chi_{r2}}{1/R+j\omega C_2} + \frac{j\omega K_{r3}\chi_{r3}}{1/R+j\omega C_3}} \tag{24}$$

The magnitude of the total voltage generated by the harvester obtained after connecting the capacitors in series across the load is given by:

$$V_T = \frac{\text{Total Charge in the Capacitors}}{\text{Equivalent Capacitance}} \tag{25}$$

Finally, the power is given by $P_T = V_T^2/R$. The formulations presented above can be extended for higher modes in doubly clamped and cantilevered harvesters as well.

III. Model Verification and Discussions

The dimensions of the harvester are chosen in a way to have a portable device with low resonant frequencies, and harvested powers in micro to milli-watt range. The length and breadth of the beam are chosen to be 140 and 25 mm, respectively, and the thicknesses of Si substructure and PZT layers are 0.5 and 0.3 mm, respectively. The mechanical damping ratio is chosen as 0.01. The beam is subjected to an acceleration of 1 m/sec^2. The total voltage and power outputs around the fundamental mode of frequency are obtained across the load resistance R.

The voltage and power variations are shown in Figs. 2 and 3, respectively. As shown in Fig. 2(a), we observe that compared to end segment (S1) the open circuit voltage generated across the mid-segment (S2) is lower. This is as expected because S2 is far away from the fixed ends, and hence, the strain

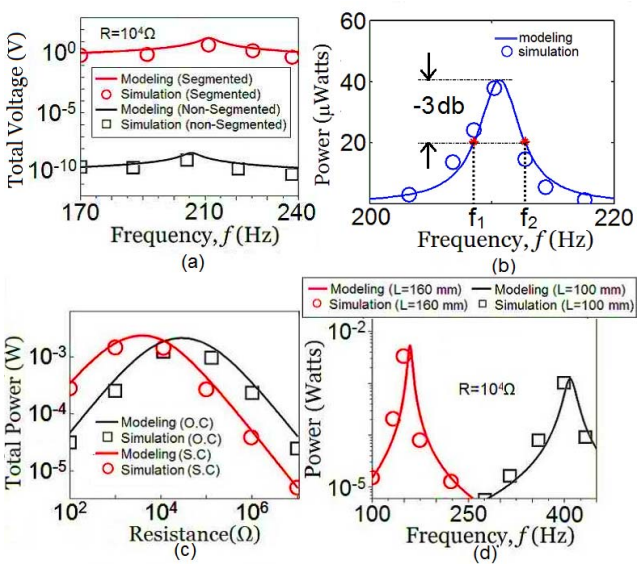

Fig. 3. (a) Total voltage of nonsegmented and segmented electrode configuration with frequency for R=10^4 Ω, (b) Total Power vs. Frequency under open circuit, (c) Total Power vs. Resistance at f_{oc} and f_{sc}, and (d) Total Power vs. Frequency for different beam lengths.

developed is also lower. On the other hand, we find from Fig. 2(b) that the charge induced in C_2 is highest. This is due to its larger area, and hence, larger C_2. The voltage output (Fig. 3(a)) for a segmented configuration is found to be greater compared to that of nonsegmented one. The external load resistance has effect on the resonant frequencies (f_c) of a piezoelectric harvester [5], [8], [11]. The existing models for harvesters with continuous electrodes does have only one capacitance $C = \epsilon_{33} bL/h_p$ associated with resistance R in the voltage equation. This C is now being replaced by C_1, C_2, and C_3 of individual segments and each of them is now separately associated with R. However, this change in capacitance configuration either by varying electrode length for continuous electrodes or by using segmented electrodes with discontinuities will affect the resonant frequency. Such shift in resonant frequency is observed in Fig. 3(a). The total power versus frequency plot for the open-circuit configuration is shown in Fig. 3(b). The model calculations for the open-circuit (OC) and short-circuit (SC) resonant frequencies f_{oc} and f_{sc}, respectively, for the beam of length L=140 mm, are found to be 211 Hz with R=10^7Ω and 205.6 Hz with R=100 Ω. When the harvester is excited at f_{oc} and f_{sc}, the total power of the harvester first increases, reaches a maximum value, and finally starts decreasing with gradual increase in resistance as shown in Fig. 3(c). These two curves intersects at a point where R=10^4 Ω. It is very interesting to note that the peaks of both the curves correspond to optimal values of load resistances of 4 kΩ and 30 kΩ, respectively, and yield almost same output power. The predictions for varying harvester length on resonant frequency are plotted in Fig. 3(d). These plots are generated for $R = 10^4$ Ω. As expected, the fundamental mode frequency decreases and harvested power increases with the increase of beam length.

Figs. 2(a) also shows the quality factor $Q = f_c/(f_2 - f_1)$ of the plots (voltage across C_2), where f_1, and f_2

are -3 dB frequencies. We have found an acceptable vale of 50 for the Q-factor. The -3 dB points for the voltage across C_1 are not shown to maintain the plot clarity. However, the same is also shown for the power plot in Fig. 3(b).

We observe from the comparative plots in Figs. 2-3 that the model calculations agree well with the Finite Element Method results. However, there is a little overestimation in the resonant frequencies. This is due to the effects of neighboring vibration modes [8] which is ignored in our single mode approximation.

IV. Conclusion

We proposed a model to study the electromechanical coupling in a piezoelectric harvester with segmented electrodes. Comparison of the model and FEM results show that the model is capable to predict the coupling effects. Although fundamental mode is considered in this study, the model can be applied for segmented doubly clamped as well as cantilevered harvesters for all modes of vibration with varying strain node positions and numbers.

References

[1] F. Khameneifar, S. Arzanpour, and M. Moallem, "A piezoelectric energy harvester for rotary motion applications: Design and experiments," *IEEE/ASME Trans. Mechatronics*, vol. 18, no. 5, pp. 1527–1534, Oct. 2013. DOI: 10.1109/TMECH.2012.2205266

[2] S. R. Anton and H. A. Sodano, "A review of power harvesting using piezoelectric materials (2003–2006)," *Smart Mater. Struct.*, vol. 16, no. 3, pp. R1–R21, Jun. 2007.

[3] Y. Zheng, X. Wu, M. Parmar, and D.-W. Lee, "Note: High-efficiency energy harvester using double-clamped piezoelectric beams," *Rev. Sci. Instrum.*, vol. 85, no. 2, pp. 026101-1–026101-3, Feb. 2014.

[4] A. Erturk, P. A. Tarazaga, J. R. Farmer, and D. J. Inman, "Effect of strain nodes and electrode configuration on piezoelectric energy harvesting from cantilevered beams," *ASME J. Vibrat. Acoust.*, vol. 131, no. 1, pp. 011010-1–011010-11, Feb. 2009.

[5] A. Erturk and D. J. Inman, "A distributed parameter electromechanical model for cantilevered piezoelectric energy harvesters," *ASME J. Vibrat. Acoust.*, vol. 130, no. 4, pp. 041002-1–041002-15, Aug. 2008.

[6] G.-Q. Wang and Y.-M. Lu, "An improved lumped parameter model for a piezoelectric energy harvester in transverse vibration," *Shock Vibrat.*, vol. 2014, Feb. 2014, Art. ID 935298.

[7] H. A. Sodano, G. Park, and D. J. Inman, "Estimation of electric charge output for piezoelectric energy harvesting," *Strain*, vol. 40, no. 2, pp. 49–58, May 2004.

[8] A. Erturk and D. J. Inman, *Piezoelectric Energy Harvesting*. Chichester, U.K.: Wiley, 2011.

[9] A. Erturk and D. J. Inman, "On mechanical modeling of cantilevered piezoelectric vibration energy harvesters," *J. Intell. Mater. Syst. Struct.*, vol. 19, no. 11, pp. 1311–1325, Nov. 2008. DOI: 10.1177/1045389X07085639

[10] S. B. Ayed, A. Abdelkefi, F. Najar, and M. R. Hajj, "Design and performance of variable-shaped piezoelectric energy harvesters," *J. Intell. Mater. Syst. Struct.*, vol. 25, no. 2, pp. 174–186, Jan. 2014. DOI: 10.1177/1045389X13489365

[11] A. Abdelkefi, N. Barsallo, L. Tang, Y. Yang, and M. R. Hajj, "Modeling, validation, and performance of low-frequency piezoelectric energy harvesters," *J. Intell. Mater. Syst. Struct.*, vol. 25, no. 12, pp. 1429–1444, Aug. 2014. DOI: 10.1177/1045389X13507638

[12] X. Xiong and S. O. Oyadiji, "Modal optimization of doubly clamped base-excited multilayer broadband vibration energy harvesters," *J. Intell. Mater. Syst. Struct.*, vol. 26, no. 16, pp. 2216–2241, Nov. 2015. DOI: 10.1177/1045389X14551433

[13] V. Dorzhiev, A. Karami, P. Basset, F. Marty, V. Dragunov, and D. Galayko, "Electret-free micromachined silicon electrostatic vibration energy harvester with the Bennet's doubler as conditioning circuit," *IEEE Electron Device Lett.*, vol. 36, no. 2, pp. 183–185, Feb. 2015.

[14] H. Liu, Y. Qian, N. Wang, and C. Lee, "An in-plane approximated nonlinear MEMS electromagnetic energy harvester," *J. Microelectromech. Syst.*, vol. 23, no. 3, pp. 740–749, Jun. 2014. DOI: 10.1109/JMEMS.2013.2281736

[15] W. Weaver, Jr., S. P. Timoshenko, and D. H. Young, *Vibration Problems in Engineering*. New York, NY, USA: Wiley, 1974.

[16] M. Paz, *Structural Dynamics: Theory and Computation*, 2nd ed. New Delhi, India: CBS Publishers, 2004, pp. 424–432.

[17] C.-C. Wu and C.-S. Chen, "An electromechanical model for a clamped–clamped beam type piezoelectric transformer," *Microsyst. Technol.*, vol. 18, no. 11, pp. 1771–1778, Nov. 2012. DOI: 10.1007/s00542-012-1495-z